Results in Physics 6 (2016) 811–816

Contents lists available at ScienceDirect

Results in Physics

journal homepage: www.journals.elsevier.com/results-in-physics

Dielectric properties of $TbMnO_3$ ceramics doped with Bi and Fe ions

Jianxun Xu, Yimin Cui *, Huaizhe Xu *

Key Laboratory of Micro-nano Measurement-Manipulation and Physics (Ministry of Education), Department of Physics, Beihang University, Beijing 100191, China

ARTICLE INFO

Article history:
Received 19 September 2016
Received in revised form 21 October 2016
Accepted 25 October 2016
Available online 26 October 2016

Keywords:
Perovskite structure
Bi doped $TbMnO_3$
Conduction progress
Dielectric response

ABSTRACT

The ceramic composites of $TbMnO_3$, $Tb_{0.95}Bi_{0.05}MnO_3$, $Tb_{0.9}Bi_{0.1}MnO_3$ and $Tb_{0.9}Bi_{0.1}Mn_{0.95}Fe_{0.05}O_3$ were compounded by conventional solid-state reaction. Both dielectric constants (ε') and loss tangent ($\tan\delta$) of composites have been measured and studied as a function of the temperature from 80 to 400 K and the frequency from 100 Hz to 1 MHz. Interestingly, doping Bi makes dielectric constant decrease and the dielectric dissipation peaks disappear in the high temperature range. But the dielectric constant becomes larger and the dielectric dissipation peaks appear again in the high temperature range after Fe doping appropriately. Analysis indicates that the perovskite structures gradually vary with the increase of Bi replacing Tb, thus the dielectric properties could be enhanced with the small amount of Mn replacement with Fe.

Introduction

Currently, studies on transition metal oxide have attracted researchers' attention due to their potential applications in recent years [1–3]. Among all the known materials, $TbMnO_3$, a typical multiferroic perovskite, shows obvious relaxations at high and low temperature with different mechanisms, respectively [4–6]. It can be applied in information storage, sensors and other new devices [7–11]. Therefore, the single characteristic of $TbMnO_3$ is supposed to be improved by partly replacing ions in Tb or Mn site such as Na, Ti, Al, Ca, Ga, Fe and La, and the origination of the high dielectric constant is discussed from the extrinsic effects, such as contact effect, spatial inhomogeneity and internal barrier layer capacitor (IBLC) [12–18]. However, the composite of Bi-doped is rarely reported, and the reported works are focus on the magnetic properties at low temperature. Golosovsky et al. [19] has proved that the low-level replaced compound $Tb_{0.95}Bi_{0.05}MnO_3$ partially suppresses the intrinsic long-range magnetic order in the Tb sublattice, and then the short-range order forms. It was shown that the propagation vector at T_{Tb} disappears in $TbMnO_3$. Zhang et al. [20] has reported that the effect of A-site Bi-doping in $TbMnO_3$, in which the structural, magnetic and dielectric properties were investigated at the low temperature range. It was found that the Bi partial replacement restrains the Tb-spin ordering point (T_{Tb}) and ferroelectric ordering point (T_C).

In our recent work, we found that physical properties are remarkably changed in Fe-doped $TbMnO_3$ [17]. Because the radius of Tb ion is similar to the Bi ion, and the radius of Mn is similar to the Fe ion, respectively. In order to maintain the stability of the perovskite structure, the Bi and Fe ion will replace the Tb- and Mn-site when doping appropriately. Then, the samples of $TbMnO_3$, $Tb_{0.95}Bi_{0.05}MnO_3$, $Tb_{0.9}Bi_{0.1}MnO_3$ and $Tb_{0.9}Bi_{0.1}Mn_{0.95}Fe_{0.05}O_3$ were fabricated by conventional solid-state reaction method. The dielectric properties of four samples have been measured and studied from 80 to 400 K. Our results reveal that the dielectric properties of $Tb_{1-x}Bi_xMnO_3$ can be improved by doping Fe.

Experiment

Polycrystalline samples $TbMnO_3$, $Tb_{0.95}Bi_{0.05}MnO_3$, $Tb_{0.9}Bi_{0.1}MnO_3$ and $Tb_{0.9}Bi_{0.1}Mn_{0.95}Fe_{0.05}O_3$ were compounded by the conventional solid-state reaction method with high-purity (>99.99%) raw powders of Tb_4O_7, MnO_2, Bi_2O_3, and Fe_2O_3. The powders were mixed and grounded in an agate mortar and sintered at 1050 °C in air for 12 h repeatedly. Then the disk samples with 8 mm in diameter and 1.5 mm in thickness were pressed. After sintered at 1100 °C in air for another 12 h, a cooling-down treatment to room temperature with furnace was followed before the end of process. Employing Cu Kα radiations as the X-ray source, the samples were characterized by X-ray diffraction (XRD) at room temperature. Micro-structural analyses were measured by scanning electron microscopy (SEM). Temperature dependent dielectric properties (capacitances and dielectric loss) were tested using a QuadTech ZM2353 LCR Digibridge in a frequency range of

* Corresponding authors.
E-mail addresses: cuiym@buaa.edu.cn (Y. Cui), hzxu@buaa.edu.cn (H. Xu).

http://dx.doi.org/10.1016/j.rinp.2016.10.018
2211-3797/

40 Hz–200 kHz, and frequency dependent dielectric properties were performed using a Precision Impedance Analyzer 6500B in a frequency range of 100 Hz–1 MHz. Electrodes on both sides of the samples were painted by the silver paste.

Results and discussion

The XRD patterns of the prepared four samples are shown in Fig. 1. Compared with the parent $TbMnO_3$, the crystalline phases of the low content doped composite $Tb_{0.95}Bi_{0.05}MnO_3$ shows almost the same patterns, which testifies this samples are mainly single phase. However, high proportion Bi-doped composites ($Tb_{0.9}Bi_{0.1}MnO_3$ and $Tb_{0.9}Bi_{0.1}Mn_{0.95}Fe_{0.05}O_3$) show miscellaneous peaks evidently, especially at 27° (2θ), marked as stars, which are the patterns of additional phases of Bi_2O_3 or BiO. So, we may safely conclude the perovskite structure is destroyed to some extent, and will find the critical doping amount of Bi replaced Tb between 5% and 10% in our next work.

The typical scanning electron micrographs are expounded in Fig. 2. The doped samples $Tb_{0.95}Bi_{0.05}MnO_3$ shows typical perovskite structure compared with the $TbMnO_3$, and the other samples, $Tb_{0.9}Bi_{0.1}MnO_3$ and $Tb_{0.9}Bi_{0.1}Mn_{0.95}Fe_{0.05}O_3$, which may be caused by the additional phases of Bi_2O_3, have the crystallization of other types observed in circles.

Fig. 3 shows the dependence of dielectric constants (ε') and loss ($\tan\delta$) with temperature for the four samples at 1, 10 and 100 kHz, respectively. In Fig. 3(a), the dielectric constants of all the samples are independence with temperature in the low temperature. When the temperature rises to 150 K, the dielectric constants of all samples begin to increase gradually. The dielectric constant of $Tb_{0.9}Bi_{0.1}Mn_{0.95}Fe_{0.05}O_3$ increases quickly, which is significantly higher than the other three samples from 200 K. With the temperature increasing, the high dielectric properties of $TbMnO_3$ gradually emerge, and its dielectric constant is larger than the other doped samples when the temperature over 300 K. But when the temperature rises to 350 K, the dielectric constant of $TbMnO_3$ keeps constant and forms a huge plateau, which numerical value is close to 10^4. With the increasing of frequency, in Fig. 3(b and c), the curves keep the same form but shift to high temperature.

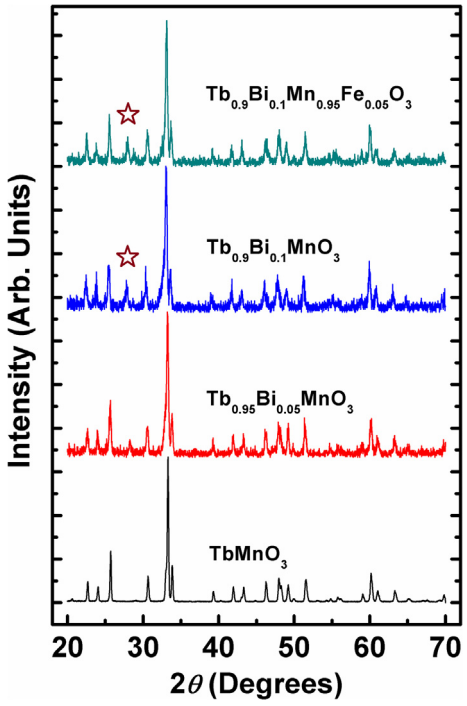

Fig. 1. The XRD patterns for $TbMnO_3$, $Tb_{0.95}Bi_{0.05}MnO_3$, $Tb_{0.9}Bi_{0.1}MnO_3$ and $Tb_{0.9}Bi_{0.1}Mn_{0.95}Fe_{0.05}O_3$.

In Fig. 3(d–f), all the dielectric loss also has an increasing tendency with increasing temperature, and the remarkable relaxations, which also shift to high temperature with the increase of frequency, can be observed in all samples at low temperature, and the relaxations of all samples are ~1 at these frequencies. However, only $TbMnO_3$ and $Tb_{0.9}Bi_{0.1}Mn_{0.95}Fe_{0.05}O_3$ can observe the relaxation at high temperature. In the Bi-doped samples, the dielectric loss of Bi-doped 10% samples ($Tb_{0.9}Bi_{0.1}MnO_3$ and $Tb_{0.9}Bi_{0.1}Mn_{0.95}Fe_{0.05}O_3$) are larger than Bi-doped 5% sample ($Tb_{0.95}Bi_{0.05}MnO_3$), which may be caused by the crystallization of other types as mentioned before. Particularly, Bi-doped 10% and Fe-doped 5% sample ($Tb_{0.9}Bi_{0.1}Mn_{0.95}Fe_{0.05}O_3$) have the same numerical value of $\tan\delta$ with the Bi-doped 5% sample ($Tb_{0.95}Bi_{0.05}MnO_3$) when the temperature rises to 360 K at 100 kHz.

The dependence of dielectric constants and loss on temperature in a range from 80 to 400 K for the four samples are pictured in Fig. 4 and Fig. 5, respectively. In Fig. 4, the samples show numerical growth in ε' with the increasing temperature followed by the appearance of a board peak at the characteristic temperature, which is strongly influenced by the frequency. At the same temperature, the dielectric constants decrease apparently with the increasing frequency. Two or three dielectric plateaus, between which the dielectric constants boost steeply, are formed at low and high temperature in all samples. This is a typical example of thermally activated Debye-like behavior. At low temperature, the coalescence of small clusters makes the size of the microdomains increase and the relaxation process makes the electric dipoles freeze, so the carriers are condensed and they cannot hop again. At the same time, there presents a decay in polarization in regard to the applied electric field, which is the demonstration of the promptly drop in ε' [21]. The electric dipoles become unfrozen with the increasing temperature. At high temperature range, the localized holes lead to conductivity through the hopping, and the dipolar effect and considerable polarization occur meanwhile, so we can get the large values of ε' when the temperature rises to 280 K [13], and the surface layer effect makes the produce of Maxwell-Wagner relaxation. The parent sample $TbMnO_3$ has large dielectric constants at high temperature ($\sim 10^4$), but the dielectric constants of Bi-doped ones are less than 10^3. Besides, the dielectric constant becomes larger ($\sim 10^3$) after adding a moderate amount of Fe, which demonstrates that the dielectric properties can be improved by doping Fe.

The temperature dependent of the dielectric loss ($\tan\delta$) are shown in Fig. 5. It is worth mentioning that the dielectric loss of all samples has an augment relationship with increasing temperature and there are some wide dielectric dissipation peaks in low temperature range (150 K–250 K), which emerges at the characteristic temperatures consistent with the drastic changes in ε'. Later, the significant difference is found in dielectric loss with temperatures increasing. The dielectric dissipation peaks of $TbMnO_3$ are quite clear in the high temperature range (280 K–400 K). However, after mixed with Bi, the dielectric loss of $Tb_{0.95}Bi_{0.05}MnO_3$ and $Tb_{0.9}Bi_{0.1}MnO_3$ increase quickly in the high temperature range, and no dielectric dissipation peaks are observed. What's more, after replace Mn with a moderate amount of Fe, the dielectric dissipation peaks of $Tb_{0.9}Bi_{0.1}Mn_{0.95}Fe_{0.05}O_3$ appear again in the high temperature range. The dielectric loss increase rapidly at the low frequency range, and dielectric dissipation are remarkable under the high frequency test with the peak of 2, which is much smaller than the peak of 4 of $TbMnO_3$ in high temperature range. As the frequency increasing, the temperature of the dissipation peaks shift to high temperature range, which show the thermally excited relaxation process, and this phenomenon can be attributed to the

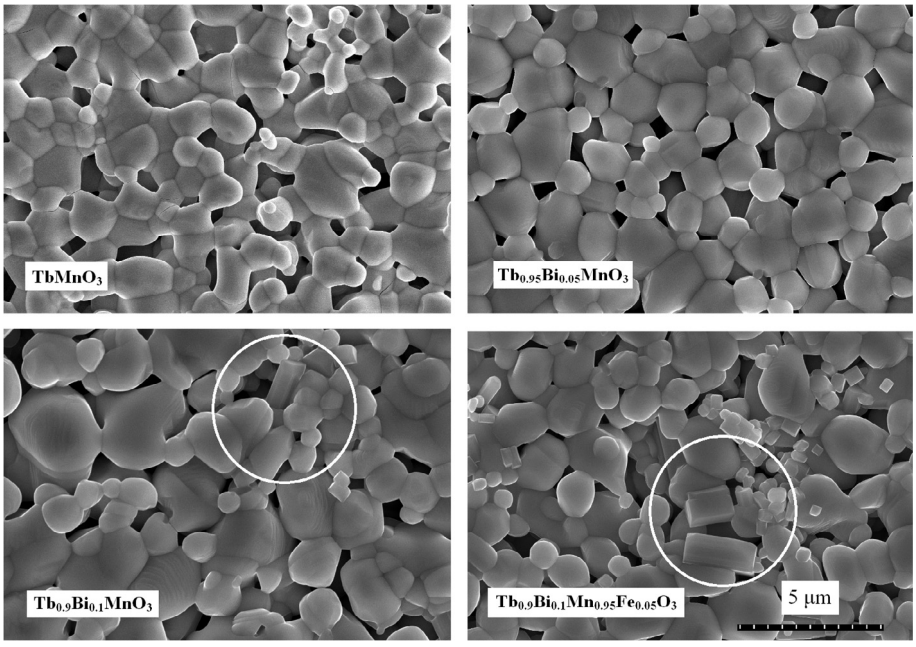

Fig. 2. The typical SEM of the polycrystalline $TbMnO_3$, $Tb_{0.95}Bi_{0.05}MnO_3$, $Tb_{0.9}Bi_{0.1}MnO_3$ and $Tb_{0.9}Bi_{0.1}Mn_{0.95}Fe_{0.05}O_3$.

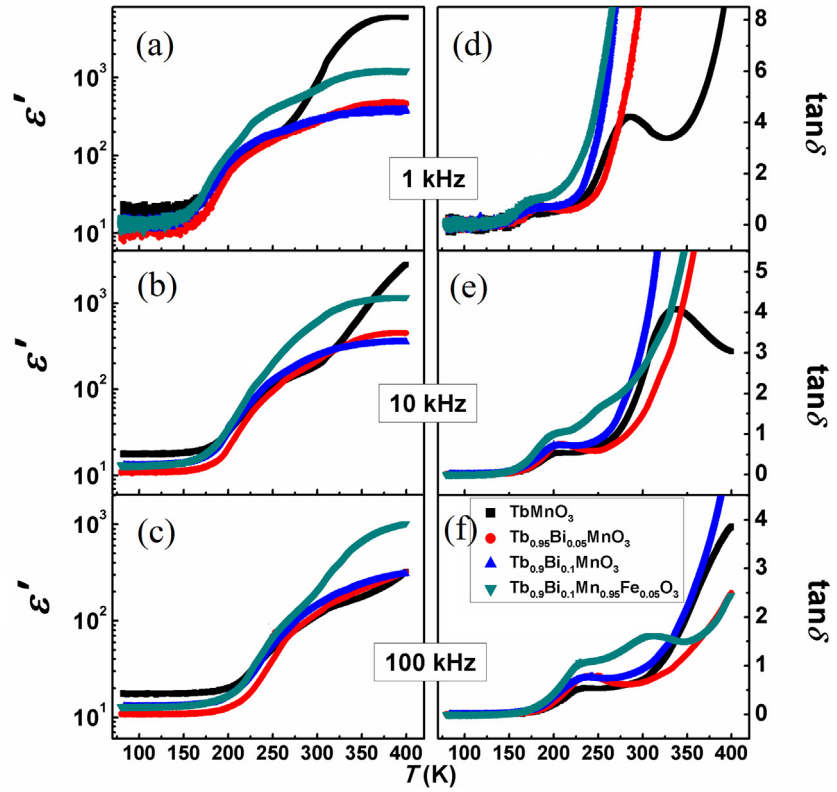

Fig. 3. The temperature dependence of (a–c) the dielectric constant (ε') and (d–f) the dielectric loss ($\tan\delta$) of four composites at 1, 10, and 100 kHz, respectively.

direct current conductivity. It is clear that the influence of the direct current conductivity is more significant with increasing temperature and decreasing frequency.

Fig. 6 shows the measured frequency versus the reciprocal of the low temperature peak position, and the obtained τ follows approximately the Arrhenius law

$$\tau = \tau_0 \exp[E/(k_B T)] \quad (1)$$

where τ and τ_0 are the relaxation time and pre-exponential factor, the energy E is the activation energy, k_B is the Boltzmann constant whose value is $1.3806488 \times 10^{-23}$ J/K and T is the absolute temperature whose unit is Kelvin. The activation energy of four samples can be calculated and shown in Table 1. It is noticeable that, compared with the parent $TbMnO_3$, Fe doping can lower the activation in low temperature range, and improve the activation in high temperature range.

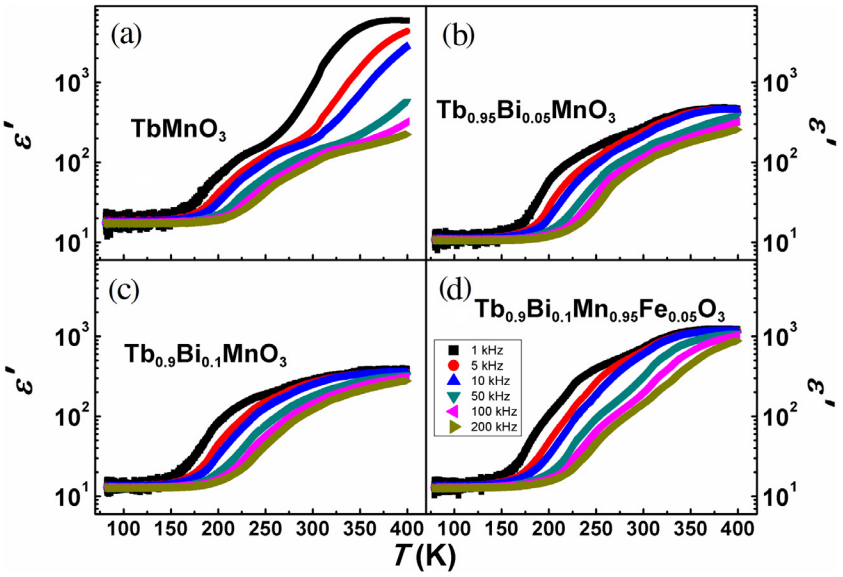

Fig. 4. The temperature dependence of the dielectric constant (ε') of (a) $TbMnO_3$, (b) $Tb_{0.95}Bi_{0.05}MnO_3$, (c) $Tb_{0.9}Bi_{0.1}MnO_3$ and (d) $Tb_{0.9}Bi_{0.1}Mn_{0.95}Fe_{0.05}O_3$ at 1, 5, 10, 50, 100 and 200 kHz, respectively.

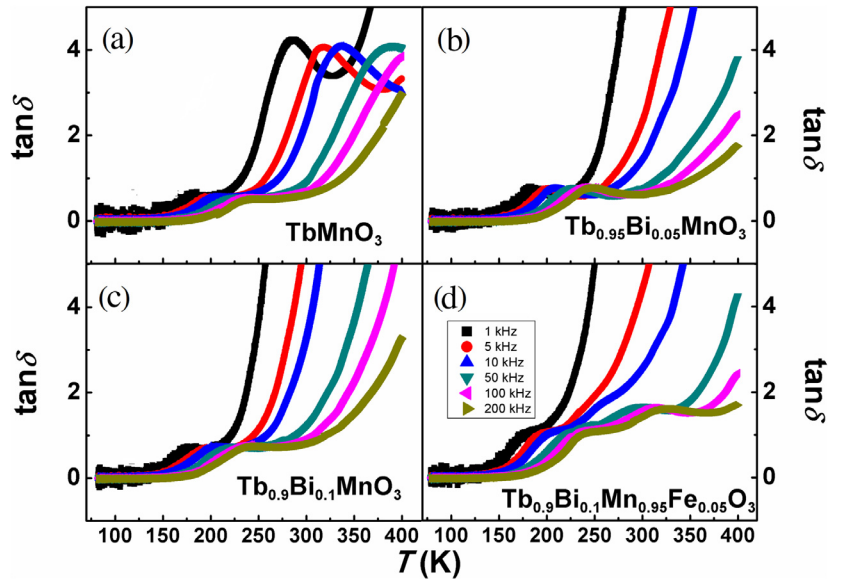

Fig. 5. The temperature dependence of the dielectric loss ($\tan\delta$) of (a) $TbMnO_3$, (b) $Tb_{0.95}Bi_{0.05}MnO_3$, (c) $Tb_{0.9}Bi_{0.1}MnO_3$ and (d) $Tb_{0.9}Bi_{0.1}Mn_{0.95}Fe_{0.05}O_3$ at 1, 5, 10, 50, 100 and 200 kHz, respectively.

Fig. 7 shows the dependence of real (ε' and imaginary (ε'') parts, where $\varepsilon'' = \varepsilon' \cdot \tan\delta$, of the complex permittivity and $\tan\delta$ of $Tb_{0.9}Bi_{0.1}Mn_{0.95}Fe_{0.05}O_3$ dependence of the frequency at different temperature from 100 to 300 K. Most curves drop nonlinearly as the temperature increasing in Fig. 7(a), and below 130 K the nearly horizontal lines in the figures manifest the dielectric constants are independence with frequencies. The dielectric loss ($\tan\delta$) decreases with increasing frequency and show distinct dielectric dissipation peaks, which appear at the characteristic frequencies corresponding to the sharp changes in ε', and the values to measurement are about 1. However, most data of $\tan\delta$ and ε'' fall on straight line partly or wholly in the frequency range covered, which manifests the conductivity has dominant contribution to ε'' [22], and the curves deviate from the straight when the temperature below 170 K as a result of the condensation of the polarized clusters in Fig. 7(c). At the low temperature range, the condensation of small clusters in samples renders the size of micro-domains to grow while the hopping carriers reduce, and the delay of the response to the external alternating field are due to the slow dynamics of the domain walls, particularly at the high frequencies range [23].

It is clearly seen in Fig. 8 that the temperature dependence of the resistivity for the four samples. The resistivity of each sample drops linearly as temperature increasing, and they are all semiconductor features. Compared with the parent $TbMnO_3$, the $Tb_{0.95}Bi_{0.05}MnO_3$ has the larger resistivity, but the resistivities of $Tb_{0.9}Bi_{0.1}MnO_3$ and $Tb_{0.9}Bi_{0.1}Mn_{0.95}Fe_{0.05}O_3$ are less than not doped samples, especially the resistivity of $Tb_{0.9}Bi_{0.1}Mn_{0.95}Fe_{0.05}O_3$ is the minimum. After doped a small amount of Bi, we think, there is no change in structure and surface morphology, and the sample of $Tb_{0.95}Bi_{0.05}MnO_3$ is still a perovskite structure. Dying to the low valence of Bi replace Tb appropriately, and in order to balance the overall valence, some Mn^{3+} change into Mn^{4+} in the Mn^{3+}/Mn^{4+}

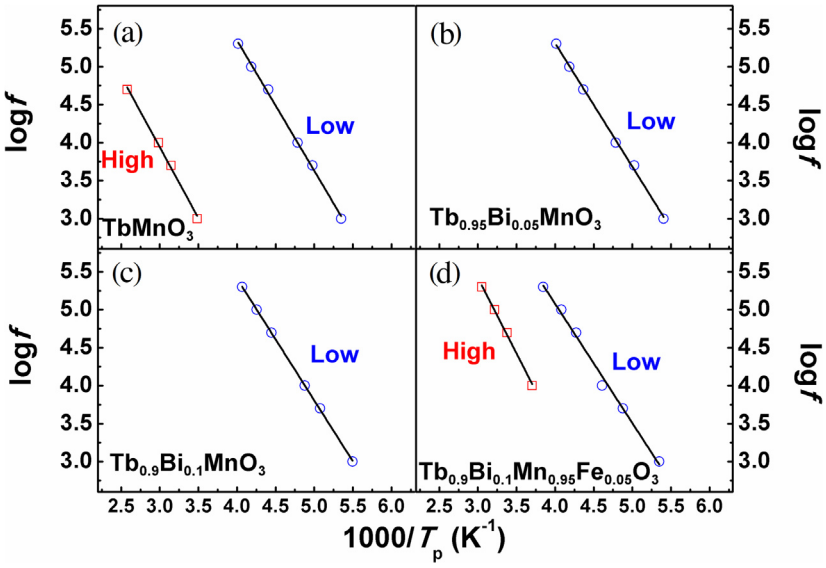

Fig. 6. The Arrhenius plots for the low and high temperature relaxation of (a) $TbMnO_3$, (b) $Tb_{0.95}Bi_{0.05}MnO_3$, (c) $Tb_{0.9}Bi_{0.1}MnO_3$ and (d) $Tb_{0.9}Bi_{0.1}Mn_{0.95}Fe_{0.05}O_3$.

Table 1
The values of activation energy of $TbMnO_3$, $Tb_{0.95}Bi_{0.05}MnO_3$, $Tb_{0.9}Bi_{0.1}MnO_3$ and $Tb_{0.9}Bi_{0.1}Mn_{0.95}Fe_{0.05}O_3$ in low and high temperature.

	$TbMnO_3$	$Tb_{0.95}Bi_{0.05}MnO_3$	$Tb_{0.9}Bi_{0.1}MnO_3$	$Tb_{0.9}Bi_{0.1}Mn_{0.95}Fe_{0.05}O_3$
E(eV) low temperature	0.336	0.329	0.319	0.312
E(eV) high temperature	0.374	–	–	0.395

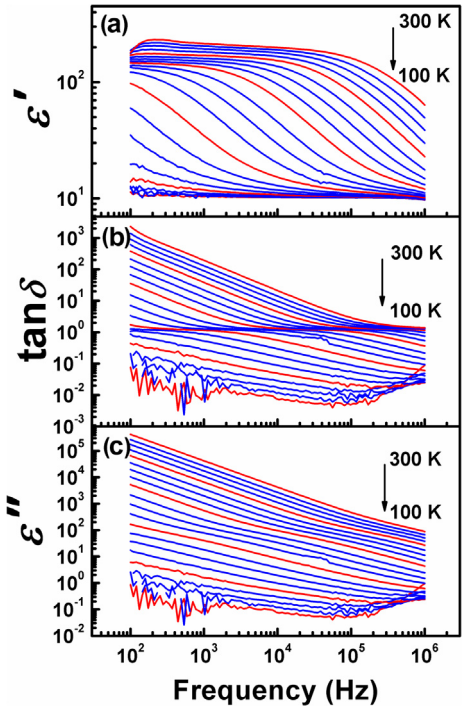

Fig. 7. The frequency dependence of (a) the real parts of the complex permittivity ε', (b) the dielectric loss $\tan\delta$ and (c) the imaginary parts of the complex permittivity ε'' of $Tb_{0.9}Bi_{0.1}Mn_{0.95}Fe_{0.05}O_3$ at fixed temperature from 100 to 300 K.

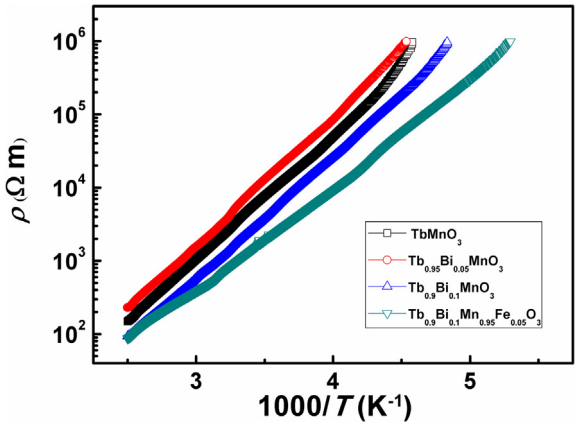

Fig. 8. The temperature dependence of the resistivity of $TbMnO_3$, $Tb_{0.95}Bi_{0.05}MnO_3$, $Tb_{0.9}Bi_{0.1}MnO_3$ and $Tb_{0.9}Bi_{0.1}Mn_{0.95}Fe_{0.05}O_3$.

structure, which reduces the Jahn-Teller ion, and makes the crystal symmetry improve, so the resistivity turns larger. When Bi doping excessively, the crystal structure is destroyed, and there is a new phase, which increases the conductivity and reduces the resistivity. The sample of $Tb_{0.9}Bi_{0.1}Mn_{0.95}Fe_{0.05}O_3$ has the minimum resistivity indicates that Fe doping appropriately can enhance the conductivity.

Complex electrical impedance is represented as: $Z^* = Z' - Z''$, in which Z', the real part of electrical impedance, is resistive component and Z'', the imaginary part, is the reactive component respectively [24]. Fig. 9 shows the impedance spectra (Nyquist plots) for the three doped samples at 180 and 300 K. To the plots, the presence of single semicircular arcs indicates that the electrical processes arise due to the contribution from grain material and two semicircular arcs indicate the contribution from both grain and grain boundary affects [25,26]. At 180 K, it is easy to observe semicircular arcs at the higher frequency (left part) in all the three samples. Only the curve of $Tb_{0.9}Bi_{0.1}Mn_{0.95}Fe_{0.05}O_3$ shows a semicircular arc at the lower frequency (right part), and the other two

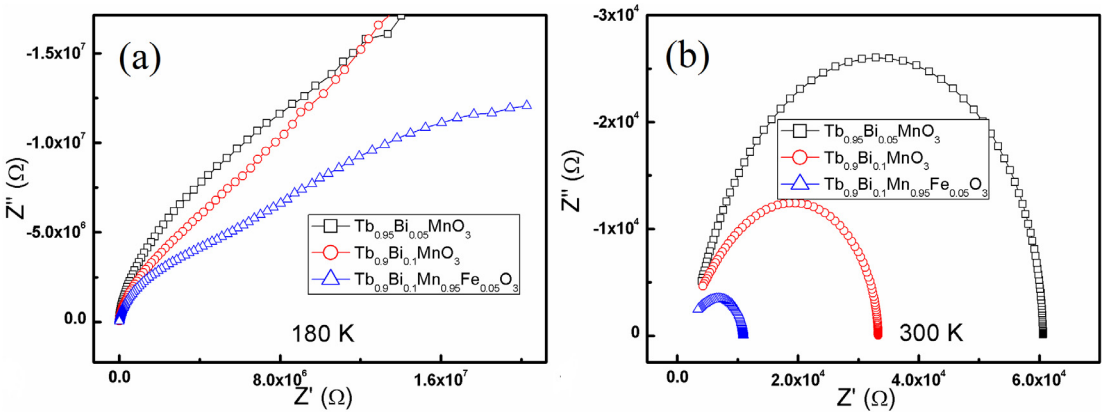

Fig. 9. Nyquist plots of $Tb_{0.95}Bi_{0.05}MnO_3$, $Tb_{0.9}Bi_{0.1}MnO_3$ and $Tb_{0.9}Bi_{0.1}Mn_{0.95}Fe_{0.05}O_3$ at (a) 180 K and (b) 300 K, respectively.

samples, $Tb_{0.95}Bi_{0.05}MnO_3$ and $Tb_{0.9}Bi_{0.1}MnO_3$, exhibit linear lines which means that $Tb_{0.9}Bi_{0.1}Mn_{0.95}Fe_{0.05}O_3$ possesses the smallest resistivity aligned with the results observed in Fig. 8. Therefore, it is found that both grain and grain boundary affect the electrical processes at 180 K, and the leading function comes from the grain boundary. When the temperature rises to 300 K, three distinct semicircular arcs can be observed, and the radius of arcs enlarges as the increasing of the resistivity. The semicircular arcs hardly appear at the higher frequency which indicates that only the dielectric responses from grain boundaries can be detected.

Conclusion

In summary, through the solid-state reaction of doping Bi and Fe ion into $TbMnO_3$, the ceramic samples have been synthesized. XRD and SEM patterns indicate that the additional phases appear in the high Bi content samples ($Tb_{0.9}Bi_{0.1}MnO_3$ and $Tb_{0.9}Bi_{0.1}Mn_{0.95}Fe_{0.05}O_3$). In the four samples, two or three remarkable dielectric plateaus can be observed at low and high temperature range respectively, between which curves of dielectric constant ε' boost sharply and shift to high temperature as frequency increasing. After mixed with Bi, the dielectric constants of $Tb_{0.95}Bi_{0.05}MnO_3$ and $Tb_{0.9}Bi_{0.1}MnO_3$ decrease but the loss of them increase quickly in the high temperature range, and no dielectric dissipation peaks are observed. However, after replace Mn with a moderate amount of Fe, the dielectric constant becomes larger ($\sim 10^3$) and the dielectric dissipation peaks reappear in the high temperature range, which indicates that the dielectric properties can be improved by doping Fe.

Acknowledgement

We acknowledge the financial support from the National Natural Science Foundation of China (No. 51331002) and (No. 51571006).

References

[1] Matsumoto Y, Murakami M, Shono T, Hasegawa T, Fukumura T, Kawasaki M, Ahmet P, Chikyow T, Koshihara S, Koinuma H. Room-temperature ferromagnetism in transparent transition metal-doped titanium dioxide. Science 2001;291:854–6.
[2] de la Cruz C, Huang Q, Lynn JW, Li JY, Ratcliff W, Zarestky JL, Mook HA, Chen GF, Luo JL, Wang NL, Dai PC. Magnetic order close to superconductivity in the iron-based layered $LaO_{1-x}F_xFeAs$ systems. Nature 2008;453:899–902.
[3] Tokura Y, Nagaosa N. Orbital physics in transition-metal oxides. Science 2000;288:462–8.
[4] Kenzelmann M, Harris AB, Jonas S, Broholm C, Schefer J, Kim SB, Zhang CL, Cheong SW, Vajk OP, Lynn JW. Magnetic inversion symmetry breaking and ferroelectricity in $TbMnO_3$. Phys Rev Lett 2005;95:087206.
[5] Goto T, Kimura T, Lawes G, Ramirez AP, Tokura Y. Ferroelectricity and giant magnetocapacitance in perovskite rare-earth manganites. Phys Rev Lett 2004;92:257201.
[6] Cui YM, Zhang LW, Wang CC, Xie GL. Strain-assisted tunneling current through $TbMnO_3$/Nb-1 wt%-doped $SrTiO_3$ p-n junctions. Appl Phys Lett 2005;86:203501.
[7] Aliouane N, Argyriou DN, Strempfer J, Zegkinoglou I, Landsgesell S, Zimmermann MV. Field-induced linear magnetoelastic coupling in multiferroic $TbMnO_3$. Phys Rev B 2006;73:020102.
[8] Senff D, Link P, Hradil K, Hiess A, Regnault LP, Sidis Y, Aliouane N, Argyriou DN, Braden M. Magnetic excitations in multiferroic $TbMnO_3$: evidence for a hybridized soft mode. Phys Rev Lett 2007;98:137206.
[9] Goto T, Yamasaki Y, Watanabe H, Kimura T, Tokura Y. Anticorrelation between ferromagnetism and ferroelectricity in perovskite manganites. Phys Rev B 2005;72:220403.
[10] Wang CC, Cui YM, Zhang LW. Dielectric properties of $TbMnO_3$ ceramics. Appl Phys Lett 2007;90:012904.
[11] Han JT, Huang YH, Huang W, Goodenough JB. Selective synthesis of $TbMn_2O_5$ nanorods and $TbMnO_3$ micron crystals. J Am Chem Soc 2006;128:14454–5.
[12] Yang CC, Wu CM, Li WH, Chan TS, Liu RS, Chen YY, Avdeev M. Effects of oxygen deficiency on the magnetic ordering of Mn in $Tb_{0.9}Na_{0.1}MnO_{2.9}$. J Phys Condens Mater 2008;20. 104234.
[13] Cui YM. Decrease of loss in dielectric properties of $TbMnO_3$ by adding TiO_2. Phys B 2008;403:2963–6.
[14] Izquierdo JL, Astudillo A, Bolaños G, Zapata VH, Morán O. Dielectric response of Al-substituted multiferroic $TbMnO_3$ at high temperatures. Ceram Int 2015;41:1285–96.
[15] Staruch M, Jain M. Long-range magnetic ordering in bulk $Tb_{1-x}M_xMnO_3$ (M = Ca, Sr). J Phys Condens Mater 2013;25:296005.
[16] Xu JX, Cui YM. Dielectric characteristics of Ga doped $TbMnO_3$. Mater Sci Eng B 2013;178:316–20.
[17] Xu JX, Cui YM, Xu HZ. Improvements of dielectric properties of Fe doped $TbMnO_3$. Ceram Int 2014;40:12193–8.
[18] Blasco J, Cuartero V, Garcia J, Rodriguez-Velamazan JA. The transition from ferromagnet to cluster-glass in $La_{1-x}Tb_xMn_{1/2}Sc_{1/2}O_3$. J Phys Condens Mater 2012;24:076006.
[19] Golosovsky IV, Mukhin AA, Ivanov VY, Vakhrushev SB, Golovenchits EI, Sanina VA, Hoffmann JU, Feyerherm R, Dudzik E. Neutron powder diffraction and single crystal X-ray magnetic resonant and non-resonant scattering studies of the doped multiferroic $Tb(Bi)MnO_3$. Eur Phys J B 2012;85:103.
[20] Zhang C, Yan HT, Wang XF, Kang DW, Li LB, Lu XM, Zhu JS. Effect of A-site Bi-doping on the magnetic and electrical properties in $TbMnO_3$. Mater Lett 2013;111:147–9.
[21] Lin YH, Li M, Nan CW, Li JF, Wu JB, He JL. Grain and grain boundary effects in high-permittivity dielectric NiO-based ceramics. Appl Phys Lett 2006;89:032907.
[22] Cui YM, Zhang LW, Xie GL, Wang RM. Magnetic and transport and dielectric properties of polycrystalline $TbMnO_3$. Solid State Commun 2006;138:481–4.
[23] Wang CC, Cui YM, Xie GL, Chen CP, Zhang LW. Phase separation in La_2CuO_{4+y} ceramics probed by dielectric measurements. Phys Rev B 2005;72:064513.
[24] Ram M. Electrical characterization of $LiCo_{3/5}Fe_{2/5}VO_4$ ceramics. Solid State Sci 2009;11:1206–10.
[25] Das PR, Choudhary RNP, Samantray BK. Diffuse ferroelectric phase transition in $Na_2Pb_2Sm_2W_2Ti_4Nb_4O_{30}$ ceramics. Mater Chem Phys 2007;101:228–33.
[26] Ram M. Transport phenomena in the compound: $LiFe_{1/2}Mn_{1/2}VO_4$. Solid State Ionics 2008;178:1922–9.